ChemPubSoc Europe

DOI: 10.1002/cphc.201801010

CHEMPHYSCHEM Articles

Excited-State Dynamics of $[Ru(bpy)_3]^{2+}$ Thin Films on Sensitized TiO_2 and ZrO_2

Valentina Leandri,[a] Peng Liu,[a] Azar Sadollahkhani,[a] Majid Safdari,[a] Lars Kloo,[a] and James M. Gardner*[a]

The excited state dynamics of Tris(2,2′-bipyridine)ruthenium(II) hexafluorophosphate, $[Ru(bpy)_3(PF_6)_2]$, was investigated on the surface of bare and sensitized TiO_2 and ZrO_2 films. The organic dyes LEG4 and MKA253 were selected as sensitizers. A Stern–Volmer plot of LEG4-sensitized TiO_2 substrates with a spin-coated $[Ru(bpy)_3(PF_6)_2]$ layer on top shows considerable quenching of the emission of the latter. Interestingly, time-resolved emission spectroscopy reveals the presence of a fast-decay time component (25 ± 5 ns), which is absent when the anatase TiO_2 semiconductor is replaced by ZrO_2. It should be specified that the positive redox potential of the ruthenium complex prevents electron transfer from the $[Ru(bpy)_3(PF_6)_2]$ ground state into the oxidized sensitizer. Therefore, we speculate that the fast-decay time component observed stems from excited-state electron transfer from $[Ru(bpy)_3(PF_6)_2]$ to the oxidized sensitizer. Solid-state dye sensitized solar cells (ssDSSCs) employing MKA253 and LEG4 dyes, with $[Ru(bpy)_3(PF_6)_2]$ as a hole-transporting material (HTM), exhibit 1.2% and 1.1% power conversion efficiency, respectively. This result illustrates the possibility of the hypothesized excited-state electron transfer.

1. Introduction

Approximately four decades ago, several researchers observed that the lowest energy excited state of several ruthenium (II) octahedral coordination complexes exhibited long lifetimes in solutions. Ruthenium(II) complexes formed with chelating diimine ligands, such as bipyridine and phenanthroline, have been particularly subjected to extensive research due to their rich photophysics and photochemistry.[1–4] Furthermore, their interesting properties made them excellent candidates for many applications. The electrogenerated chemiluminescence (ECL) of tris-chelated ruthenium(II) complexes has been successfully exploited in the generation of light-emitting diodes (LEDs), organic light-emitting diodes (OLEDs) and light-emitting electrochemical cells (LECs).[5–8] Efficient quenching of the triplet excited state of these complexes via energy transfer to produce singlet oxygen, made them efficient oxygen sensors.[9] Moreover, their characteristic absorption in the visible portion of the electromagnetic spectrum, as well as their redox properties, led to excellent results in the field of water splitting.[10–13] However, it was within the field of dye-sensitized solar cells (DSSCs) in which, perhaps, ruthenium(II) complexes of the type discussed above have been more extensively employed. Due to their aforementioned strong visible light absorption and their redox properties, ruthenium(II) polypyridyl complexes quickly emerged as outstanding photosensitizers for DSSCs and maintained their supremacy for more than 20 years.[14–19] Another interesting application of such complexes was as energy relay dyes (ERDs) for DSSCs. In the latter case, the purpose was to exploit the pore volume of mesoporous TiO_2 for light harvesting by ERDs in devices based on a solid-state (hole-transporting material) HTM or a liquid electrolyte. In a second step, the energy harvested through ERDs light absorption was then transferred to a sensitizer anchored on the surface of TiO_2 via resonance energy transfer. Inspired by a work of Siegers and colleagues,[20] Nazeeruddin et al. successfully extended the concept from liquid to solid-state dye-sensitized solar cells (ssDSSCs) by introducing a ruthenium(II) sensitizer as ERD inside the hole transporting layer.[21] These results triggered subsequent extensive research on the topic.[22–26] Surprisingly, the literature only focuses on the Förster resonant energy transfer (FRET) between the ERD and the sensitizer, and other possible interactions are not taken into account. Moreover, there is no existing record of a spectroscopic investigation performed at the direct interface of ERDs and sensitizers. Therefore, our goal is to study the excited state dynamics of thin films of a ruthenium(II) complex employed as ERD which is deposited on the surface of non-sensitized and sensitized TiO_2 and ZrO_2 mesoporous layers. In particular, tris(2,2′-bipyridine)ruthenium (II) hexafluorophosphate, $[Ru(bpy)_3](PF_6)_2]$, was selected as an ERD while the organic dyes LEG4 and MKA253, well known for their good performances in DSSCs,[27–30] were chosen as sensitizers. The excited state dynamics of $Ru(bpy)_3^{2+}$ have been explored through steady-state and time-resolved spectroscopies. Furthermore, we fabricated and characterized ssDSSCs

[a] Dr. V. Leandri, Dr. P. Liu, Dr. A. Sadollahkhani, Dr. M. Safdari, Prof. L. Kloo, Prof. J. M. Gardner
Department: Department of Chemistry
Division of Applied Physical Chemistry
KTH Royal Institute of Technology
Teknikringen 30, SE-10044, Stockholm, Sweden
E-mail: jgardner@kth.se

Supporting information for this article is available on the WWW under https://doi.org/10.1002/cphc.201801010

in which $[Ru(bpy)_3](PF_6)_2]$ was employed a HTM. Our results interestingly suggest that a photoinduced electron transfer from the excited state of $Ru(bpy)_3^{2+}$ to the oxidized sensitizers could potentially be a mechanism involved in the excited state quenching observed on mesoporous TiO_2 films. We propose that such electron transfer could become a viable regeneration mechanism of the oxidized sensitizers and be exploited for future optimization of hybrid and organic solar cells.

2. Results and Discussion

The structures of LEG4 and MKA253 dyes are shown in the Supporting Information (Figure S1). Steady-state spectroscopy measurements were performed to evaluate any interaction at the interfaces dye/$[Ru(bpy)_3]^{2+}$ and TiO_2/$[Ru(bpy)_3]^{2+}$. The electronic absorption and emission spectra for ruthenium tris (bipyridine) films on TiO_2, in the absence of dye, are displayed in Figure 1.

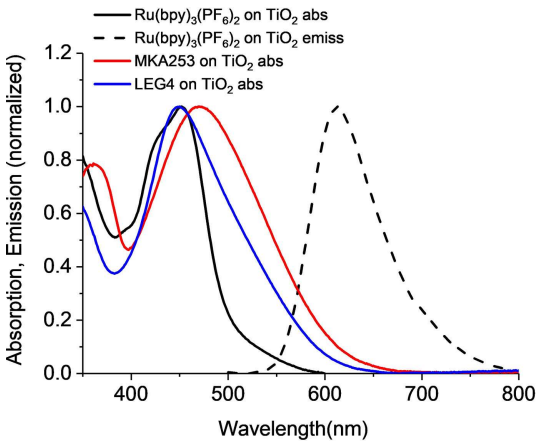

Figure 1. Normalized room temperature absorption (black solid line) and emission (dashed line) spectra of a $Ru(bpy)_3(PF_6)_2$ film spin coated on TiO_2 substrates. Excitation wavelength used: 450 nm. Normalized absorption spectra of dyes MKA253 (red solid line) and LEG4 (blue solid line) absorbed on TiO_2 films.

The absorption spectrum reveals a structured peak with an absorption maximum at $\lambda = 452$ nm, which has been assigned to a metal-to-ligand (d–π*) charge transfer (MLCT) process.[31] On the other hand, the emission spectrum from the $[Ru(bpy)_3]^{2+}$ triplet excited-state is essentially unstructured and displays a maximum intensity at $\lambda = 613$ nm. These results show minimal or no deviation from the absorption and emission spectra of the same ruthenium complex in solution.[31,32] The photoluminescence (PL) of an emissive molecule may be completely or partially quenched by interactions with molecules or materials that can accept energy or electrons from the emissive molecule's excited-state. Figure 2 displays the steady-state photoluminescence quenching of the $[Ru(bpy)_3]^{2+}$ triplet excited-state upon increasing the concentration of the dye LEG4 on the TiO_2 surface. The change in dye load/

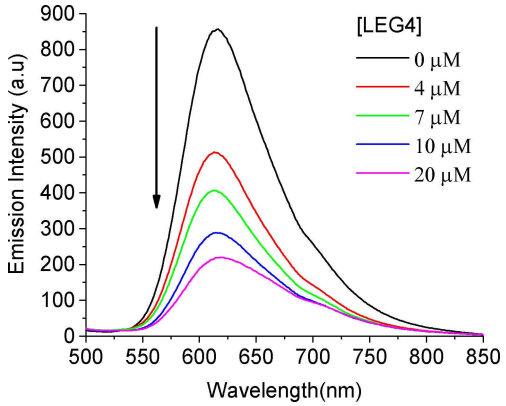

Figure 2. Photoluminescence intensity of $Ru(bpy)_3(PF_6)_2$ films spin coated on TiO_2 substrates with varying amount of the dye LEG4 adsorbed on the semiconductor surface. The concentration reported in the legend refers to the concentration of the dye-bath used to sensitize the electrodes (see Samples Preparation section for more details). Each spectrum was obtained by averaging the emissive response from 3 different samples. Excitation wavelength used:450 nm.

concentration was achieved by varying the dye-bath concentrations. For simplicity, the following detailed spectroscopic investigation is based on the dye LEG4 exclusively, although similar photoluminescence quenching was observed for MKA253 as well (Figure S2).

There are numerous types of quenching mechanisms that can be responsible for the decrease of the observed emission.[33–35] A plot of the relative luminescence intensity as a function of the quencher concentration, also known as Stern–Volmer plot, is a useful tool to investigate the types of mechanisms dominating the quenching process. In a control experiment we have calculated the Stern–Volmer plot also for ZrO_2 films, as the relatively high conduction band edge of this material prevents electron injection from the dye or $*[Ru(bpy)_3]^{2+}$.[36,37] Therefore, any difference observed between the Stern–Volmer plots obtained for the two different substrates can provide insights on the quenching mechanisms occurring. Figure 3 shows the Stern-Volmer plots obtained from the steady-state photoluminescence measurement in Figure 2 with LEG4 dye adsorbed onto TiO_2, and from the analogous system on ZrO_2 films (Figure S4). The linearity of the relationship between the PL intensity and the quencher concentration observed in both cases suggests that one main type of quenching mechanism is predominant. Equation (1) shows the Stern-Volmer relation for static and dynamic quenching:

$$\frac{I_0}{I} = 1 + K_{sv}[Q] \quad (1)$$

Where I_0 and I are the PL intensities in the absence and presence of quencher, respectively; K_{sv} is the Stern–Volmer quenching constant, and $[Q]$ is the concentration of the quencher.

The quenching constants (K_{sv}) obtained in our systems are equal to 48 M^{-1} (on TiO_2) and 21 M^{-1} (on ZrO_2). These values are

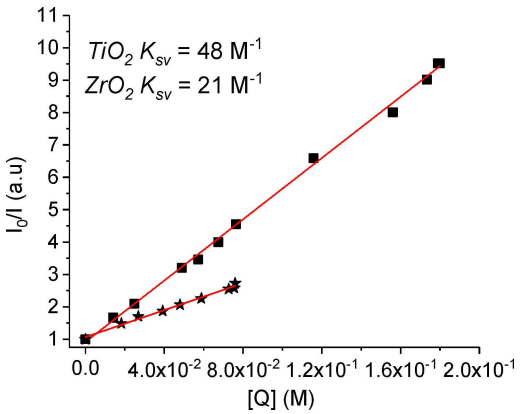

Figure 3. Stern-Volmer plot of emission quenching of $Ru(bpy)_3(PF_6)_2$ films by the dye LEG4 on TiO_2 (black squares) and ZrO_2 (black stars). The [Q] value was calculated from the Beer-Lambert law using the absorbance of the dye on the semiconductor substrates, the molar extinction coefficient calculated in solution, and the thickness of the TiO_2 and ZrO_2 substrates (500 nm).The emission intensity from $Ru(bpy)_3(PF_6)_2$ was monitored at $\lambda = 613$ nm.

several orders of magnitude lower than many others reported in the literature. However, the vast majority of the systems investigated do not involve a solid-solid interface but instead typically one phase in which the quencher is free to diffuse, such as vapor or liquid.[31,38] In a study by Tyagi et al., the quenching of tris(8-hydroxyquinolinato)aluminium (Alq_3) by 2,3,5,6-tetrafluoro-7,7′,8,8′-tetracyano quinodimethane (F_4-TCNQ) in a pure solid-state system was reported to have a K_{sv} of 13.8 M^{-1}, which is of the same order of magnitude as our results.[39] This may suggest that, when both the donor and the quencher are restricted in the solid state, the observed quenching constants may be lower due to the limited diffusion in an essentially immobilized system. The calculated quenching constants with the LEG4 dye adsorbed on mesoporous titanium oxide and zirconium oxide are within the same order of magnitude. Interestingly, less efficient quenching is observed for the samples in which the dye has been absorbed on zirconium oxide. This observation suggests the presence of one or more quenching mechanisms which occur when the dye is absorbed on the TiO_2 substrates, but not when it is on ZrO_2 films. In order to have a clearer view of the possible underlying mechanism, or mechanisms, we analyze the quenching pathways which may occur on the different semiconductor surfaces. After excitation (equation 2), we identify 4 main possible quenching mechanisms [Equations (3)–(6)] on ZrO_2:

$$ZrO_2/D \xrightarrow{h\nu} ZrO_2/D^* \; ; \; [Ru(bpy)_3] \xrightarrow{h\nu} {}^*[Ru(bpy)_3]^{2+} \quad (2)$$

$$ZrO_2/D^* + {}^*[Ru(bpy)_3]^{2+} \rightarrow ZrO_2/D^* + [Ru(bpy)_3]^{2+} \quad (3)$$

$$ZrO_2/D^* + {}^*[Ru(bpy)_3]^{2+} \rightarrow ZrO_2/D^- + [Ru(bpy)_3]^{3+} \quad (4)$$

$$ZrO_2/D^* + {}^*[Ru(bpy)_3]^{2+} \rightarrow ZrO_2/D^+ + [Ru(bpy)_2(bpy)^-] + \quad (5)$$

$$ZrO_2/\{D[Ru(bpy)_3]^{2+}\} \xrightarrow{h\nu} ZrO_2/\{D[Ru(bpy)_3]^{2+}\}^* \quad (6)$$

$${}^*[Ru(bpy)_3]^{2+} + 3O2 \rightarrow [Ru(bpy)_3]^{2+} + 1O2 \quad (7)$$

It is already well known from the literature which successfully employs ruthenium (II) complexes as ERDs, that energy transfer from its excited state $*[Ru(bpy)_3]^{2+}$ to dye molecules (D) in their ground state is a viable quenching mechanism [Equation (3)]. Other possible mechanisms involve an electron transfer between the two species in their excited states [Equations (4) and (5)]. However, if such an electron transfer occurs,[40][41] it has to be within the lifetime of the excited state of the dye (D^*). Intermolecular photoinduced electron-transfer processes can take place even on a picosecond or sub-picosecond timescale if the involved species are in close contact,[42–45] and do not represent a rate-limiting step. However, the electron-transfer processes in the reactions (4–5) imply that the two excited-states involved in the process must coexist at a relatively short distance within the time frame of a few nanoseconds,[37,46] and such conditions are rare and are only likely to occur at high photon fluxes. Furthermore, a quenching mechanism in which the dye and the ruthenium complex form an association complex in the ground state (static quenching) which is non-fluorescent is described in Equation (6). Finally, oxygen quenching, independent from the type of metal oxide employed as substrate, is represented in Equation (7).

On the other hand, dyes adsorbed on a semiconductor with relatively low conduction band energies, such as TiO_2, can readily undergo oxidation by photoinduced electron transfer into the conduction band (CB) of the semiconductor as shown in Equations (8) and (9).

$$TiO_2/D \xrightarrow{h\nu} TiO_2/D^* \quad (8)$$

$$TiO_2/D^* \rightarrow (e_{CB})TiO_2/D^+ \quad (9)$$

Having the oxidized form of the dye (D^+) on the semiconductor surface, allows new photochemistry to occur. Apart from the quenching mechanisms discussed on ZrO_2 [(Equations (3)–(6)] which can take place on TiO_2 as well, and oxygen quenching [Equation (7)], the additional quenching mechanism involves electron transfer from the excited state of the ruthenium (II) complex to the oxidized dye [Equation (10)]:

$$TiO_2/D^+ + {}^*[Ru(bpy)_3]^{2+} \rightarrow TiO_2/D + [Ru(bpy)_3]^{3+} \quad (10)$$

This quenching pathway can potentially be of significant impact. Indeed, transient-absorption measurements have shown that in the case of dyes bound to mesoporous TiO_2, the timescale for charge recombination between the electrons in the conduction band (CB) of TiO_2 ($e_{CB}(TiO_2)$) and the oxidized dye molecules adsorbed on the surface (TiO_2/D^*) occurs on the μs-ms time scale.[47][48][36] Therefore, photoinduced electron-transfer reactions to the oxidized dye on TiO_2 [Equation (10)] are statistically more probable than the electron transfer processes reported in equations 4 and 5.

In order to acquire more insights on the quenching mechanism, time-resolved photoluminescence (TRPL) measurements were performed. The results are presented in Figure 4. In agreement with the steady-state measurements, the intensity of the photoluminescence from the ruthenium complex films decreases progressively as the concentration of the dye on the

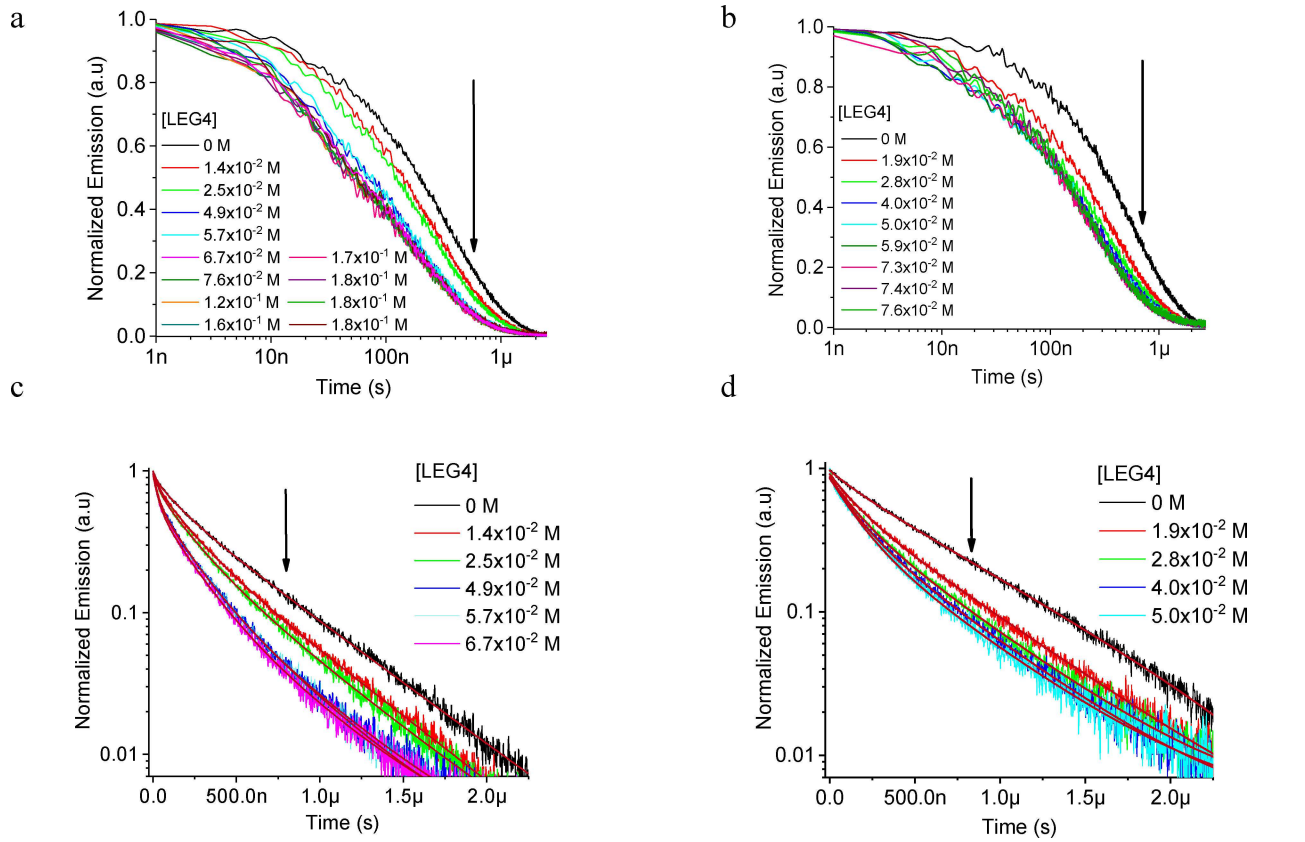

Figure 4. (a) TRPL kinetic traces of samples with a $Ru(bpy)_3(PF_6)_2$ film spin coated on top of TiO_2 substrates sensitized with different concentrations of the dye LEG4; (b) TRPL kinetic traces of samples with a film of $Ru(bpy)_3(PF_6)_2$ spin coated on top of ZrO_2 substrates sensitized with different concentrations of the dye LEG4; (c) Logarithmic decay of the normalized TPRL kinetic traces reported in (a). TRPL profiles for concentrations 20–0.130 μM overlap and are not shown in the graph for clarity (Figure S6); (d) Logarithmic decay of the normalized TPRL kinetic traces reported in (b). TRPL profiles for higher concentrations overlap and are not shown for clarity (Figure S6). The dark red lines (c-d) show the data fitting. Excitation wavelength used = 532 nm; observed emission wavelength used = 625 nm. Every trace shown represents an average of 3 traces obtained from different samples. LEG4 concentration was calculated from the Beer-Lambert law using the absorbance of the dye on the semiconductor substrates, the molar extinction coefficient calculated in solution, and the thickness of the TiO_2 and ZrO_2 substrates (500 nm).

TiO_2/ZrO_2 surface increases. Furthermore, as LEG4 is adsorbed on the semiconductor surfaces, the normalized decay traces plotted on a logarithmic scale (Figure 4c–d) reveal a significant deviation from the decay of the non-sensitized samples. This deviation is already evident at very low dye loading and stabilizes for samples obtained from dye-bath concentrations >10 μM (Figure S6). As seen from Figure 4c–d, the photoluminescence quenching is dynamic in origin; the traces change not only in intensity but in shape as well. The photoluminescence from $[Ru(bpy)_3]^{2+}$ on ZrO_2 substrates decays exponentially, and a simple model consisting of a sum of two exponential components is sufficient to describe the decay profiles. Figure 5 collects the results from the fitted model to the normalized time-resolved photoluminescence data (Figure 4) recorded for mesoporous ZrO_2 and TiO_2. As mentioned previously, the energy of the conduction band edge of ZrO_2 is more negative than the excited-states of both $[Ru(bpy)_3]^{2+}$and LEG4. The high energy band edge inhibits charge injection into ZrO_2 and the formation of $LEG4^+$ or $[Ru(bpy)_3]^{3+}$. As a consequence, we do not expect any time component related to the electron transfer from $*[Ru(bpy)_3]^{2+}$ to the oxidized dye. The populations of excited states that describe the decay profiles are those located at the air/$Ru(bpy)_3^{2+}$ and ZrO_2/dye/$Ru(bpy)_3^{2+}$ interfaces. On ZrO_2, we assign the time constant τ_2, to the natural lifetime of $*[Ru(bpy)_3]^{2+}$. In absence of the dye on ZrO_2, the natural lifetime is observed, plus quenching (τ_1) that may be due to oxygen [Equation (7)]. This suggests that the excited states population related to the τ_1 component resides at the air/$[Ru(bpy)_3]^{2+}$ interface. As LEG4 is bound to ZrO_2, fewer $*[Ru(bpy)_3]^{2+}$ are in contact with ZrO_2 and more come into contact with the dye. Consequently, the pre-exponential factor associated with the natural lifetime decreases. In response to the presence of the dye bound to ZrO_2, the natural lifetime decreases due to differences in the dielectric constant between ZrO_2 and the dye; the $*[Ru(bpy)_3]^{2+}$ feels a different electronic environment when the dye is present. As the value and pre-exponential factor for τ_2 decreases, the pre-exponential factor for the time constant τ_1 increases. However, the photoluminescence decay from $*[Ru(bpy)_3]^{2+}$ on TiO_2 substrates is more complex. The simplest and adequate fit to the data is based on the sum of three exponential functions, as shown in Equation (11).

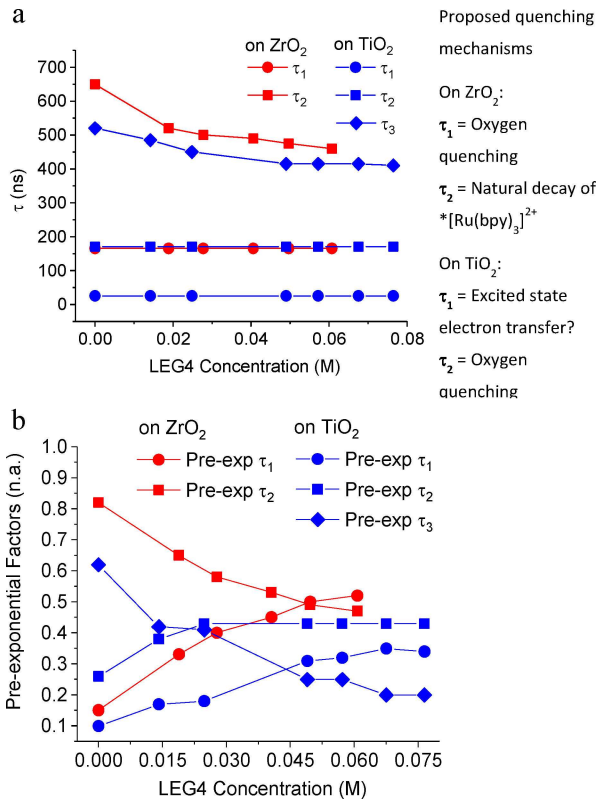

Figure 5. Lifetimes in nanoseconds (a) and weights of the pre-exponential factors (b) of the decay components relative of the luminescence spectra of $[Ru(bpy)_3]^{2+}$ spin coated on mesoporous non-sensitized/sensitized ZrO_2 (red dots and squares) and TiO_2 (blue dots, squares and diamonds) films. LEG4 concentration was calculated from the Beer-Lambert law using the absorbance of the dye on the semiconductor substrates, the molar extinction coefficient calculated in solution, and the thickness of the TiO_2 and ZrO_2 substrates (~500 nm). Excitation wavelength used = 532 nm. Emission intensity observed at $\lambda = 620$ nm.

$$I(t) = I_1\exp(-\frac{t}{\tau_1}) + I_2\exp(-\frac{t}{\tau_2}) + I_3\exp(-\frac{t}{\tau_3}) \quad (11)$$

The observed lifetimes on TiO_2 differ by factors between 3 and 20, and the pre-exponential factors vary significantly as well. These aspects indicate that the multiexponential analysis is adequate and that at least three different non-radiative decay processes occur on TiO_2 substrates. In the absence of the dye, the shortest time component (25 ± 5 ns) has been assigned to the photoinduced electron transfer from $*[Ru(bpy)_3]^{2+}$ into the TiO_2 CB, in agreement with the literature.[49,50] Since $[Ru(bpy)_3]^{2+}$ is only physically absorbed on TiO_2, and its excited-state redox potential is extremely close to the anatase CB edge, the contribution from this quenching mechanism is small (0.1, i.e. ~10%). The mid (170 ± 5 ns) time component τ_2 on TiO_2 exhibits a lifetime that is extremely close to the observed τ_1 on ZrO_2 (160 ± 5 ns), suggesting oxygen quenching [Equation (7)]. The longer time component τ_3 (520 ± 5 ns) is very similar to the observed τ_2 on ZrO_2 (650 ± 10 ns), therefore we assign this time constant to the natural lifetime of $*[Ru(bpy)_3]^{2+}$ in the TiO_2 system. As the LEG4 dye is adsorbed on the TiO_2 surface and its concentration increases, the shorter time component remains constant at about 25 ns, which we believe to be an effect of the limitation of our instrument.

However, the pre-exponential factor of this model component increases. We believe that this may be due to the fact that the excited-state electron transfer from $*[Ru(bpy)_3]^{2+}$ to the oxidized dye [Equation (10)] also contributes to this process. This is reasonable, as quenching via photoinduced electron transfer becomes evidently more likely to occur as the concentration of the oxidized dye increases. The population of excited states that we hypothesized to be mainly quenched by oxygen retain a constant lifetime throughout the series. Finally, the population of $*[Ru(bpy)_3]^{2+}$ that naturally decays, undergoes a noticeable decrease both in lifetime (from 520 to 400 ns) and pre-exponential factor (from 0.62 to 0.20). This is, once again, consistent with our model: the decrease of population simply counterbalances the increasing population of excited states that is quenched by the mechanism reported in Equation (10).

To make sure that the energetics of the molecules involved in the discussion made so far were actually appropriate for the excited state electron transfer reported in Equation (10) to occur, we recorded the cyclic voltammetry (CV) and differential pulse voltammetry (DPV) results of $Ru(bpy)_3(PF_6)_2$ in acetonitrile solution and the dyes LEG4/MKA253 adsorbed onto TiO_2 substrates (Figure 6).

$Ru(bpy)_3(PF_6)_2$ in solution exhibits one redox peak at 0.95 V vs $Ag/AgNO_3$ (1.51 V *vs* NHE).[51] The organic sensitizers LEG4 and MKA253 adsorbed onto TiO_2 electrodes exhibit two distinct oxidation peaks, respectively, at 0.50 V and 0.76 V for LEG4 (1.05 V and 1.32 V vs NHE), and at 0.30 V and 0.66 V for MKA253 (0.85 V and 1.22 V vs NHE), in agreement with the literature.[30,52] It can be clearly seen from the electrochemical analysis that any electron transfer from the ground state of $[Ru(bpy)_3](PF_6)_2$ to the oxidized dye is energetically unfavorable due to the more negative potential of the latter. The thermodynamic driving force ($-\Delta G$) for electron transfer (i.e. dye regeneration, in this case) between $Ru(bpy)_3(PF_6)_2$ and the oxidized dye can be estimated from the redox potentials calculated from the data reported in Figure 6, according to Equation (12):

$$-\Delta G_{dye-Ru(II/III)} = ve\Delta E = ve[E_{1/2}(D^+/D) - E_{1/2}(Ru^{III}/Ru^{II})] \quad (12)$$

where $E_{1/2}$(RuIII/II) and $E_{1/2}(D^+/D)$ are the redox potentials of the $Ru(bpy)_3(PF_6)_2$ and the dye, respectively, ΔE is the potential difference between the dye and the ruthenium complex, ν is the number of electrons involved in the process, and e is the elementary charge of the electron.[53] By applying equation 12 to the results obtained from the electrochemical study displayed in Figure (6), leads to a $\Delta E = -0.46$ eV (-44 kJ mol^{-1}) in the case of LEG4 and $\Delta E = -0.66$ eV (-63 kJ mol^{-1}) for MKA253. Clearly, both energy barriers are thermodynamically inaccessible at room temperature. However, the redox potential of the ruthenium complex triplet excited-state ($*[Ru(bpy)_3]^{2+}$ /$[Ru(bpy)_3]^{3+}$; -0.57 V vs NHE),[51] provides a substantial driving force for the regeneration of both LEG4 and MKA253. Applying the redox potential for the couple *Ru(II)/Ru(III) in equation 12 leads to a $\Delta E = 1.62$ eV (156 kJ mol^{-1}) for the regeneration of

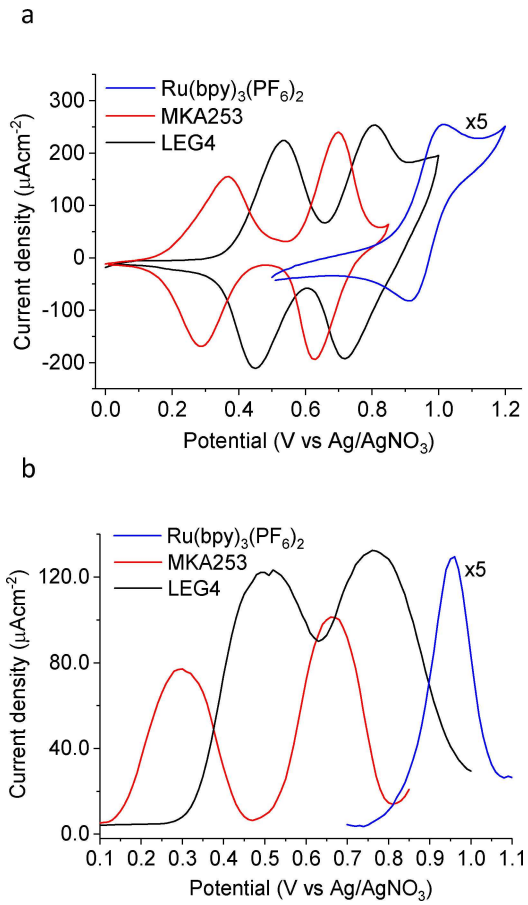

Figure 6. CV (a) and DPV (b) traces of $Ru(bpy)_3(PF_6)_2$ in acetonitrile solution (blue solid lines) and the dyes LEG4 (black solid lines) and MKA253 (red solid lines) adsorbed on TiO_2 electrodes. All the observed oxidative waves are reversible. Reference electrode $Ag/AgNO_3$. The potential of the $Fc^{+/0}$ redox couple was used as an internal standard (0.63 V vs NHE).

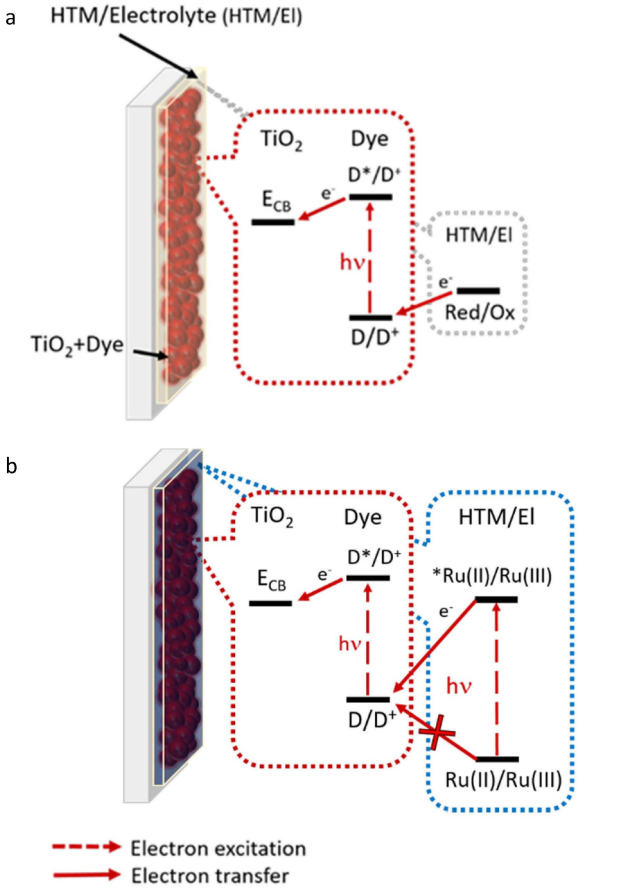

Figure 7. (a) Dye injection and dye regeneration mechanisms in a conventional DSSC,[31] and (b) in a hypothetical DSSC using $[Ru(bpy)_3](PF_6)_2$ as redox shuttle/HTM.

Table 1. Photovoltaic characteristics of DHSSCs employing $Ru[(bpy)_3](PF_6)_2$ as HTM and LEG4/MKA253 as dyes.

Dye	J_{sc} [mA cm^{-2}]	V_{oc} [mV]	FF [%]	η [%][a]
MKA253	4.39	680	42	1.2
LEG4	3.10	795	46	1.1
No Dye	0.033	625	50	0.01

[a] Under simulated 1 sun AM 1.5G illumination.

LEG4 and $\Delta E = 1.42$ eV (137 kJ mol^{-1}) for MKA253. These latter values suggest that the processes is thermodynamically very favorable and provide additional support to our previous interpretation which attributed a relevant role to the excited state electron transfer between $*[Ru(bpy)_3]^{2+}$ and the oxidized dye [Equation (10)].

If the aforementioned excited state electron transfer occurs, it could be exploited as a regeneration pathway for the oxidized dye molecules in DSSCs. Therefore, one would expect to be able to fabricate functioning photovoltaic devices using $[Ru(bpy)_3](PF_6)_2$ as either redox mediator or hole-transporting material (HTM) (Figure 7).

Consequently, we made and characterized ssDSSCs in which $[Ru(bpy)_3](PF_6)_2$ was used as HTM and the compounds LEG4 and MKA253 as dyes (Figure S7). Table 1 collects the ssDSSCs detailed photovoltaic parameter.

It is possible to notice that the fabricated solar cells are actually working and exhibit a moderate power conversion efficiency (η). This implies that the oxidized form of LEG4 is being necessarily regenerated to its neutral state by electron transfer, thus supporting our hypothesis of the mentioned excited-state electron transfer mechanism. Consistently with other studies, solar cells based on the dye MKA253 exhibit higher photocurrent density (J_{sc}) but lower open-circuit voltage (V_{oc}) as compared to those based on LEG4.[30,54] The relatively low V_{oc}, in combination with a poor fill factor (FF) suggests that the devices are most likely exposed to a high degree of charge-carrier recombination loss. This is reasonable considering that the oxidized HTM species, i.e $[Ru(bpy)_3]^{3+}$, has a very positive redox potential and can therefore act as efficient recombination center. In addition, the significant spectra overlap between the dyes and the $[Ru(bpy)_3]^{2+}$ light absorption represents a limitation. The superior performance of devices based on dye MKA253 may be related to its broader absorption of the visible spectrum (Figure S8).[30] The IPCE of the ssDSSCs based on the

dye MKA253 is reported in the Supporting Information (Figure S9). Furthermore, the contribution of direct excited-state electron transfer from $[Ru(bpy)_3]^{2+}$ into the CB of TiO_2 was assessed by fabricating devices with non-sensitized substrates in which the HTM layer was spin coated onto bare TiO_2. Such solar cells displayed a maximum efficiency of 0.01 %, excluding any significant contribution to direct electron injection from $*[Ru(bpy)_3]^{2+}$ into the CB of TiO_2 (Figure S10). We believe the power-conversion efficiencies (η) reported in Table 1 to be promising, providing a further support to the excited state electron transfer mechanism we hypothesized, and pointing in the direction of a potential new approach to dye regeneration in DSSCs.

3. Conclusions

We have investigated the excited states dynamics of a film of $[Ru(bpy)_3](PF_6)_2$ in contact with non-sensitized and sensitized (LEG4 dye) TiO_2 and ZrO_2 surfaces. The steady-state emission measurements on TiO_2 substrates sensitized with the dye LEG4 have shown remarkable quenching of the emission from $*[Ru(bpy)_3]^{2+}$. Time-resolved photoluminescence (TRPL) studies performed on the non-sensitized and sensitized TiO_2 and ZrO_2 substrates, show a dynamic quenching mechanism. Data fitting of the time-resolved profiles reveals the presence of a fast time component, at the limit of our nanosecond detection possibilities, which was present on the TiO_2-based system. The fast time component is absent when ZrO_2 is employed. A detailed analysis of the possible quenching pathways suggests that electron transfer from the excited state of $[Ru(bpy)_3]^{2+}$ to the oxidized LEG4 dye could be the mechanism appearing as fast-time component on the TiO_2 samples. Cyclic voltammetry has been employed to calculate the redox potential of $[Ru(bpy)_3]^{2+}$ in solution and of the dyes LEG4 and MKA253 on TiO_2. The results show that electron transfer from the excited state of $*[Ru(bpy)_3]^{2+}$ to oxidized LEG4 or MKA253 would be energetically favorable (156, and 137 kJ mol^{-1}, respectively), while the electron transfer from its ground state results thermodynamically unfavourable (−44, and −63 kJ mol^{-1}). Finally, we tested the hypothesis according to which if the aforementioned electron transfer mechanism was taking place, it would have been possible to fabricate functional solar cells based on $Ru(bpy)_3(PF_6)_2$ as either redox shuttle or hole-transporting material (HTM). Fabricated ssDSSCs with LEG4 and MKA253 as dyes, and $Ru[(bpy)_3](PF_6)_2$ as HTM resulted in notable efficiencies of around 1 %. Although further research is needed in order to provide direct spectroscopic evidence for the mentioned excited state electron transfer, we have provided steady-state, time-resolved, electrochemical and photovoltaic data that support that hypothesis.

Experimental Section

General

Tris(2,2′-bipyridine)ruthenium(II) hexafluorophosphate was purchased from Sigma-Aldrich and used without further purification. The organic dyes LEG4 and MKA253 were provided by Dyenamo AB and used as received. Glass substrates coated with a fluorine-doper tin oxide (FTO) layer were purchased from Pilkington. TEC15 and TEC8 were used for working electrodes and counter electrodes, respectively.

Electrochemical Characterization

Electrochemical experiments were performed in a three-electrode electrochemical cell with a platinum wire as counter electrode, Ag/$AgNO_3$ (10 mM/acetonitrile) as reference electrode, and an FTO electrode with spin-coated mesoporous TiO_2 (non-sensitized) as working electrode for the cyclic voltammetry (CV) and differential pulse voltammetry (DPV) of $Ru[(bpy)_3](PF_6)_2$ in solution. CVs and DPVs of dyes MKA253 and LEG4 on TiO_2 were performed using a sensitized TiO_2 working electrode. The supporting electrolyte used was a 0.1 M $(n\text{-}Bu)_4NPF_6$/acetonitrile solution. The measurements were performed using an Ivium Technologies vertex potentiostat. Ferrocene (Fc) was used as internal standard and the redox potentials reported considering Fc+/Fc in acetonitrile solution to be 0.63 eV *vs* NHE.

Steady-State Absorption and Emission Spectroscopy

UV-visible absorption spectra were recorded using a double-beam UV-visible Cary 300 Spectrophotometer. Emission spectra were recorded with a Cary Eclipse Fluorescence Spectrophotometer. Details about sample preparation can be found in the sample preparation section.

Time-Resolved Photoluminescence Spectroscopy

Time-resolved photoluminescence decay traces were recorded on a home-built system including a NewWave Tempest Nd:YAG laser operated at 532 nm (10 Hz, 5 mJ/pulse, FWHM = 5 ns) as an excitation source, DSO–X 2012 A oscilloscope from Agilent as the digitizing component, Thorlabs PMTSS multialkali PMT module (190–900 nm, 1.4 ns rise time) as a detector, and a Princeton Instruments monochromator (blazed at 350 nm) to select detecting wavelength. All optics and mirrors were acquired from Thorlabs. The program was written in LabView 2014. Samples were excited at 532 nm (10 Hz repetition rate) at an incident angle of 45 degrees relative to the laser pulse and 50 degrees relative to the detector. In an average measurement, 500–600 shots were averaged to collect a decay trace. The samples have been both excited and measured from the HTM side (ruthenium film) in order to avoid inner filter effects.

Sample Preparation for Steady-State and Time-Resolved Spectroscopy

Microscope slides were used for these measurements instead of the thicker Pilkington glasses with FTO in order to minimize light scattering effects. Plain microscope slides (VWR) were cut into substrates of 1.5 × 2.5 cm^2 and cleaned in an ultrasonic bath for half an hour with ethanol. A volume of 60 μl of colloidal TiO_2 (Dyesol 18NR–T:ethanol = 1:3 w/w) or ZrO_2 (Solaronix ZT-SP:ethanol = 1:3 w/w) was then spin coated (2000 rpm, 30 s) onto the clean glass

substrates. The resulting substrates were sintered by a gradient heating process: 180 °C for 10 min, 320 °C for 10 min, 400 °C for 10 min, 450 °C for half of an hour in air atmosphere. After cooling to room temperature, 3 substrates were immersed into a dye-bath solution (acetonitrile:*t*-butanol = 1:1 volume ratio, 10 ml solution volume) with an appropriate concentration of either LEG4, or MKA253, for 1 hour. The sensitized substrates were then rinsed with ethanol and dried by air flow. For the substrates which included a tris(2,2′-bipyridine)ruthenium(II) hexafluorophosphate film: 60 µl of a 10 mM solution of the ruthenium complex in acetonitrile was spin coated (2000 rpm, 30 s) on the non-sensitized/sensitized TiO_2 or ZrO_2 substrates prepared on the microscope slides.

Film Thickness Characterization

Measurements of the thickness of TiO_2 and ZrO_2 layers were made by means of a profilometer (Veeco Dektak 150).

Photovoltaic Devices Fabrication

Fluorine-doped SnO_2 (TEC15) substrates were etched with Zn powder and HCl (4 M) to form the desired electrode pattern. The substrates were cleaned in an ultrasonic bath for half an hour with the following solvents: deionized water, acetone and ethanol. A compact layer of TiO_2, intended to block the recombination current at the FTO support, was prepared on cleaned FTO substrate by spray pyrolysis. The solution used for the spray pyrolysis was composed of 0.2 M Ti-isopropoxide and 2 M acetylacetone in isopropanol and a 10-spray cycle was used as the standard procedure. A colloidal TiO_2 paste (Dyesol 18NR–T:ethanol = 1:3 w/w) was spin coated (2000 rpm, 30 s) on the compact layer surface and then sintered by a gradient heating process: 180 °C for 10 min, 320 °C for 10 min, 400 °C for 10 min, 450 °C for half of an hour (Nabertherm Controller P320) in air atmosphere. After sintering, the films were treated with 40 mM $TiCl_4$ aqueous solution at 70 °C for 30 min. After rinsing with deionized water and ethanol, the films were sintered again by following the previously mentioned procedure. After cooling to 90 °C, the films were immersed into the dye-bath solution (LEG4 or MKA253, 0.15 mM in acetonitrile:*t*-butanol, 1:1 vol. ratio) for 14 h. Subsequently, the films were rinsed in ethanol and dried by an air flow. The sensitized TiO_2 layer was covered with a tris(2,2′-bipyridine)ruthenium(II) hexafluorophosphate solution by spin coating (2000 rpm, 30 s). The solution was composed of 10 mM ruthenium complex, 200 mM 4-*tert*-butylpyridine (TBP), and 20 mM LiTFSI in acetonitrile. Finally, a 200 nm thick Ag (Sigma-Aldrich; ≥ 99.99% trace metals basis) contact layer was deposited onto the dye-sensitized TiO_2 layer by thermal evaporation, in a vacuum chamber (Leica EM MED020) with a base pressure of about 10^{-5} mbar, in order to complete the device.

Photovoltaic Devices Characterization

Current-voltage (*I-V*) measurements were carried out with a Keithley 2400 source/meter and a Newport solar simulator (Model 91160); the light intensity was calibrated using a certified reference solar cell (Fraunhofer ISE), to an intensity of 1000 $W m^{-2}$ (AM 1.5G spectrum). The devices were placed inside a mask with an aperture area of 0.126 cm^2 during the measurements. Incident photo-to-current conversion efficiency (IPCE) spectra were recorded by a computer-controlled setup comprised of a xenon lamp (Spectral Products ASB-XE-175), a monochromator (Spectral Products CM110) and a Keithley multimeter (Model 2700), calibrated by a certified reference solar cell (Fraunhofer ISE).

Acknowledgements

The Swedish Research Council, the Swedish Energy Agency and Knut & Alice Wallenberg Foundation are acknowledged for their financial support. J.G. would like to graciously acknowledge the support from the Swedish government through the strategic research area "STandUP for ENERGY".

Conflict of Interest

The authors declare no conflict of interest.

Keywords: Excited-state electron transfer · $Ru(bpy)_3$ · DSSCs · Photochemistry · Solid state

[1] C. Kaes, A. Katz, M. W. Hosseini, *Chem. Rev.* **2000**, *100*, 3553–3590.
[2] J. V. Caspar, T. J. Meyer, *J. Am. Chem. Soc.* **1983**, *105*, 5583–5590.
[3] J. M. Lehn, R. Ziessel, *J. Organomet. Chem.* **1990**, *382*, 157–173.
[4] Y. Fuchs, S. Lofters, T. Dieter, W. Shi, R. Morgan, T. C. Strekas, H. D. Gafney, A. D. Baker, *J. Am. Chem. Soc.* **1987**, *109*, 2691–2697.
[5] F. G. Gao, A. J. Bard, *J. Am. Chem. Soc.* **2000**, *122*, 7426–7427.
[6] B. Y. Tung, S. Lee, Y. Chi, L. Chen, C. Shu, F. Wu, A. J. Carty, P. Chou, S. Peng, G. Lee, *Adv. Mater.* **2005**, *17*, 1059–1064.
[7] H. J. Bolink, L. Cappelli, E. Coronado, P. Gavina, *Inorg. Chem.* **2005**, *44*, 5966–5968.
[8] R. D. Costa, E. Ortí, H. J. Bolink, F. Monti, G. Accorsi, N. Armaroli, *Angew. Chem. Int. Ed.* **2012**, *51*, 8178–8211; *Angew. Chem.* **2012**, *124*, 8300–8334.
[9] S. Ji, W. Wu, W. Wu, P. Song, K. Han, Z. Wang, S. Liu, H. Guo, J. Zhao, *J. Mater. Chem.* **2010**, *20*, 1953–1963.
[10] W. J. Youngblood, S. A. Lee, Y. Kobayashi, E. A. Hernandez-pagan, P. G. Hoertz, T. A. Moore, A. L. Moore, D. Gust, T. E. Mallouk, *J. Am. Chem. Soc.* **2009**, *131*, 926–927.
[11] D. R. Tobergte, S. Curtis, *Photochemistry and Photophysics of Metal Complexes*, **2013**.
[12] K. Hanson, D. A. Torelli, A. K. Vannucci, M. K. Brennaman, H. Luo, L. Alibabaei, W. Song, D. L. Ashford, M. R. Norris, C. R. K. Glasson, *Angew. Chem. Int. Ed.* **2012**, *51*, 12782–12785; *Angew. Chem.* **2012**, *124*, 12954–12957.
[13] B. D. Sherman, Y. Xie, M. V. Sheridan, D. Wang, D. W. Shaffer, T. J. Meyer, J. J. Concepcion, *ACS Energy Lett.* **2017**, *2*, 124–128.
[14] B. O'Regan, M. Grätzel, *Nature* **1991**, *353*, 737–739.
[15] M. K. Nazeeruddin, R. Humphry-Baker, P. Liska, M. Grätzel, *J. Phys. Chem. B* **2003**, *107*, 8981–8987.
[16] M. K. Nazeeruddin, F. De Angelis, S. Fantacci, A. Selloni, G. Viscardi, P. Liska, S. Ito, B. Takeru, D. Chimica, V. Uni, *J. Am. Chem. Soc.* **2005**, *127*, 16835–16847.
[17] M. K. Nazeeruddin, P. Péchy, T. Renouard, S. M. Zakeeruddin, R. Humphry-Baker, P. Comte, P. Liska, L. Cevey, E. Costa, V. Shklover, *J. Am. Chem. Soc.* **2001**, *123*, 1613–24.
[18] R. Buscaino, C. Baiocchi, C. Barolo, C. Medana, M. Grätzel, M. K. Nazeeruddin, G. Viscardi, *Inorg. Chim. Acta* **2008**, *361*, 798–805.
[19] J. Albero, P. Atienzar, A. Corma, H. Garcia, *Chem. Rec.* **2015**, *15*, 803–828.
[20] C. Siegers, J. Hohl-Ebinger, B. Zimmermann, U. Würfel, R. Mülhaupt, A. Hinsch, R. Haag, *ChemPhysChem* **2007**, *8*, 1548–1556.
[21] J. H. Yum, B. E. Hardin, S. J. Moon, E. Baranoff, F. Nüesch, M. D. McGehee, M. Grätzel, M. K. Nazeeruddin, *Angew. Chem. Int. Ed.* **2009**, *48*, 9277–9280; *Angew. Chem.* **2009**, *121*, 9441–9444.
[22] E. L. Unger, L. Yang, B. Zietz, G. Boschloo, *J. Photonics Energy* **2015**, *5*, 057406.
[23] M. Rahman, M. J. Ko, J. Lee, *Nanocsale* **2015**, 3526–3531.
[24] B. E. Hardin, J.-H. Yum, E. T. Hoke, Y. C. Jun, P. Péchy, T. Torres, M. L. Brongersma, M. K. Nazeeruddin, M. Grätzel, M. D. McGehee, *Nano Lett.* **2010**, *10*, 3077–3083.
[25] N. D. Eisenmenger, K. T. Delaney, V. Ganesan, G. H. Fredrickson, M. L. Chabinyc, *J. Phys. Chem. C* **2014**, *118*, 14098–14106.

[26] J. H. Yum, B. E. Hardin, E. T. Hoke, E. Baranoff, S. M. Zakeeruddin, M. K. Nazeeruddin, T. Torres, M. D. McGehee, M. Grätzel, *ChemPhysChem* **2011**, *12*, 657–661.
[27] K. Kakiage, Y. Aoyama, T. Yano, K. Oya, J. Fujisawa, M. Hanaya, *Chem. Commun.* **2015**, *51*, 15894–15897.
[28] Y. Hao, W. Yang, L. Zhang, R. Jiang, E. Mijangos, Y. Saygili, L. Hammarstro, A. Hagfeldt, G. Boschloo, *Nat. Commun.* **2016**, *7*, 1–8.
[29] V. Leandri, W. Yang, J. M. Gardner, G. Boschloo, S. Ott, *ACS Appl. Energy Mater.* **2018**, *1*, 202–210.
[30] P. Liu, B. Xu, K. M. Karlsson, J. B. Zhang, N. Vlachopoulos, G. Boschloo, L. C. Sun, L. Kloo, *J. Mater. Chem. A* **2015**, *3*, 4420–4427.
[31] S. Campagna, P. Francesco, G. Bergamini, V. Balzani, C. Inorganica, C. Analitica, *Top. Curr. Chem.* **2007**, *280*, 117–214.
[32] B. Durham, J. V. Caspar, J. K. Nagle, T. J. Meyer, *J. Am. Chem. Soc.* **1982**, *104*, 4803–4810.
[33] J. R. Lakowicz, in *Princ. Fluoresc. Spectrosc.* **2006**, pp. 277–330.
[34] A. Marton, C. C. Clark, R. Srinivasan, R. E. Freundlich, A. A. Narducci Sarjeant, G. J. Meyer, *Inorg. Chem.* **2006**, *45*, 362–369.
[35] B. E. Hardin, A. Sellinger, T. Moehl, R. Humphry-Baker, J.-E. Moser, P. Wang, S. M. Zakeeruddin, M. Grätzel, M. D. McGehee, *J. Am. Chem. Soc.* **2011**, *133*, 10662–7.
[36] S. Tatay, S. A. Haque, B. O'Regan, J. R. Durrant, W. J. H. Verhees, J. M. Kroon, A. Vidal-Ferran, P. Gavina, E. Palomares, *J. Mater. Chem.* **2007**, *17*, 3037–3044.
[37] R. Katoh, A. Furube, T. Yoshihara, K. Hara, G. Fujihashi, S. Takano, S. Murata, H. Arakawa, M. Tachiya, *J. Phys. Chem. B* **2004**, *108*, 4818–4822.
[38] F. Vögtle, M. Plevoets, M. Nieger, G. C. Azzellini, A. Credi, L. De Cola, V. De Marchis, M. Venturi, V. Balzani, *J. Am. Chem. Soc.* **1999**, *121*, 6290–6298.
[39] P. Tyagi, S. Tuli, R. Srivastava, *J. Chem. Phys.* **2015**, *142*, DOI 10.1063/1.4907274.
[40] C. Creutz, N. Sutin, *Inorg. Chem.* **1976**, *15*, 496–499.
[41] B. H. Farnum, J. M. Gardner, G. J. Meyer, *Inorg. Chem.* **2010**, *49*, 10223–10225.
[42] A. Hagfeldt, G. Boschloo, L. Sun, L. Kloo, H. Pettersson, *Chem. Rev.* **2010**, *110*, 6595–663.
[43] J. M. Rehm, G. L. McLendon, Y. Nagasawa, K. Yoshihara, J. Moser, M. Grätzel, *J. Phys. Chem.* **1996**, *100*, 9577–9578.
[44] N. S. Sariciftci, L. Smilowitz, A. J. Heeger, F. Wudl, *Science* **1992**, *258*, 1474–1476.
[45] S. Doose, H. Neuweiler, M. Sauer, *ChemPhysChem* **2009**, *10*, 1389–1398.
[46] J. S. Lissau, J. M. Gardner, A. Morandeira, *J. Phys. Chem. C* **2011**, *115*, 23226–23232.
[47] J.-H. Yum, E. Baranoff, F. Kessler, T. Moehl, S. Ahmad, T. Bessho, A. Marchioro, E. Ghadiri, J.-E. Moser, C. Yi, *Nat. Commun.* **2012**, *3*, 631.
[48] G. Boschloo, A. Hagfeldt, *Acc. Chem. Res.* **2009**, *42*, 1819–26.
[49] K. Hashimoto, M. Hiramoto, A. B. P. Lever, T. Sakata, *J. Phys. Chem.* **1988**, *92*, 1016–1018.
[50] K. Hashimoto, M. Hiramoto, T. Kajiwara, T. Sakata, *J. Phys. Chem.* **1988**, *92*, 4636–4640.
[51] C. Creutz, N. Sutin, *Inorg. Chem.* **1976**, *15*, 496–499.
[52] V. Leandri, J. Zhang, E. Mijangos, G. Boschloo, S. Ott, *"Journal Photochem. Photobiol. A Chem.* **2016**, *328*, 59–65.
[53] T. Daeneke, A. J. Mozer, Y. Uemura, S. Makuta, M. Fekete, Y. Tachibana, N. Koumura, U. Bach, L. Spiccia, *J. Am. Chem. Soc.* **2012**, *134*, 16925–16928.
[54] M. Freitag, W. Yang, L. A. Fredin, L. D. Amario, K. M. Karlsson, A. Hagfeldt, G. Boschloo, *ChemPhysChem* **2016**, *17*, 3845–3852.

Manuscript received: October 31, 2018
Revised manuscript received: January 6, 2019
Accepted manuscript online: January 8, 2019
Version of record online: February 7, 2019